AIAA SciTech Forum
6-10 January 2025, Orlando, FL
AIAA SCITECH 2025 Forum

10.2514/6.2025-0298

Numerical Investigation of Electron Energy Transport in Hall Thrusters

Declan G. Brick* Parker J. Roberts† and Benjamin A. Jorns‡
University of Michigan, Ann Arbor, Michigan, 48109

Self-consistent closures for the electron heat flux and collision frequency in a multi-fluid Hall thruster model are parametrically investigated. A form of the anomalous collision frequency that follows the scaling of the classical electron-ion collision frequency is employed. Three separate models of a free-stream heat flux along magnetic field lines are explored and compared to a classical Spitzer-Harm representation. These models are applied to a 9-kW class Hall thruster operating on xenon and krypton and compared to experimental measurements of internal plasma properties and global thruster performance. It is found that with the modified heat flux, the model is self-consistently able to capture ion velocity measurements as well as the 2D electron temperature along magnetic field lines. However, the model underpredicts peak temperature along centerline by 25% and performance metics by 35%. These results are discussed in the context of the physical significance of the freestream heat flux. The extensibility of the model is explored and shown to be able to represent changes in the ion velocity across propellant, discharge voltage, and discharge current by only adjusting a single scaling constant.

I. Nomenclature

a	=	coefficient for electron thermal conductivity along field lines
α	=	tunable coefficient for scaling the free-stream heat flux
$\vec{B}$	=	magnetic field
b	=	coefficient for electron thermal conductivity across field lines
β	=	tunable coefficient for Bohm-like profiles
c	=	tunable coefficient for scaling the anomalous collision frequency
c_w	=	tunable coefficient for scaling the electron flux to the walls
e	=	fundamental charge
$\vec{E}$	=	electric field
$\vec{j}_e$	=	electron current density
$\vec{j}_{e,th}$	=	electron thermal current density
$\vec{j}_i$	=	ion current density
κ	=	electron thermal conductivity
$ln(\Lambda)$	=	Coulomb logarithm
m	=	mass
m_e	=	electron mass
m_i	=	ion mass
n_e	=	electron number density
n_i	=	ion number density
$\dot{n}$	=	ionization source term
$\hat{n}$	=	unit vector indicating direction normal to wall
P_e	=	electron pressure
P_i	=	ion pressure
ϕ	=	electrostatic potential
$\vec{q}$	=	heat flux

*PhD Candidate, Department of Aerospace Engineering, AIAA Student Member.
†PhD Candidate, Department of Aerospace Engineering, AIAA Student Member.
‡Associate Professor, Department of Aerospace Engineering, AIAA Associate Fellow.

$q_\parallel$ = heat flux parallel to magnetic field
q_i = ion charge
Q = energy source term due to collisions
r = anomalous collision frequency relaxation factor
R_i = Drag force on ions due to collisions
T_e = electron temperature
ν_{an} = anomalous collision frequency
ν_{ei} = electron-ion collision frequency
ν_{iz} = ionization collision frequency
ν_w = electron-wall collision frequency
ν_e = total electron collision frequency
$\vec{v}$ = velocity
$\vec{v}_i$ = ion velocity
$v_{e,\parallel}$ = electron velocity parallel to magnetic field
$v_{e,th}$ = electron thermal velocity
ω_{ce} = electron cyclotron frequency
Z = charge state of ion population
$Z*$ = effective charge state of ions
z = axial position, from anode
$\hat{v}_{e,\parallel}$ = unit vector describing direction of electron velocity parallel to magnetic field
$\hat{\parallel}$ = unit vector describing direction parallel to magnetic field
$\hat{\perp}$ = unit vector describing direction perpendicular to magnetic field

II. Introduction

Predictive modeling of Hall thrusters has been a long-standing goal of the electric propulsion community due to the potential capabilities modeling-based tools offer for reducing flight qualification time and making performance extrapolations from ground-based tests to flight-like conditions. A major challenge in achieving this end, however, is that there are key aspects of the electron dynamics in Hall thrusters that are inherently kinetic effects. Self-consistently modeling these behaviors in principle requires high-fidelity kinetic modeling [1, 2] that can be computationally prohibitive for the typical timescales and geometries of real Hall thrusters [3]. In light of this limitation, reduced-fidelity treatments of the electrons such as fluid representations are the only currently viable method for practical, engineering models of Hall thrusters. These commonly take the form of multi-fluid or hybrid codes (c.f. Ref. [4]). With that said, despite the popularity and speed of these reduced fidelity representations, they inherently lose the ability to self-consistently represent the kinetic nature of the electron physics. This shortcoming poses a challenge for using these tools for predictive modeling.

With this challenge in mind, there have been several attempts to date to approximate these kinetic dynamics through closure modeling. It is common practice, for example, to introduce an effective "anomalous" collision frequency for electrons that approximates a phase-space averaged response of the the electron velocity distribution function (EVDF) to microscopic fluctuations in the plasma [5]. This additional collision frequency is then included in the calculation of both the mobility and conductivity transport coefficients [6–14]. However, adding this additional variable to the fluid system of equations introduces a closure problem. While the classical formulation of plasma fluid equations represents a closed set of tractable equations, introducing this extra collision frequency opens this series of equations.

In order to re-close these questions, a number of previous efforts have adopted a "Bohm-like" form of the collision frequency where an empirical coefficient [15] or set of coefficients [16] is multiplied by the electron cyclotron frequency. These coefficients are then adjusted until the simulation's outputs of ion velocity and performance match experimental measurement [17]. While this semi-empirical approach has resulted in simulations that can provide key insight into the internal dynamics of the thruster [18], it contains the inherent limitation that it requires existing experimental data to inform the calibration of the Bohm coefficients. These values often are unique to the operating condition and device, precluding them from being extensible and limiting their predictive capability.

As an alternative to this semi-empirical approach, multiple efforts have focused on exploring first-principles closure of the anomalous collision frequency [19–29]. These models are derived based on hypotheses about the underlying processes that drive the transport. Examples include wall collisions [19, 20], onset of turbulence [24, 25], shear suppression of turbulence [21–23], and wave driven instabilities [26–28]. These closure models share the common

feature that they self-consistently depend on fluid properties and thus provide an additional governing equation. To date, however, no self-consistent closure model has proved fully predictive.

Arguably, one of the major challenges in finding a first-principles model is in the common belief that the anomalous collision frequency in the thruster is highly non-linear with respect to position. Past experimental and modeling efforts have suggested that the Bohm coefficient varies by three to four orders of magnitude over a length scale smaller than the thruster length scale[17, 27, 30]. This variation is necessary to provide the transport barrier to drive the steep axial electric field profiles that have been observed in these devices [31]. With that said, none of the bulk fluid properties in the discharge exhibit this high level of variation, which makes deriving a first-principles closure challenging. Some proposed closures have attempted to resolve this issue by introducing exponential dependencies on electron quantities, which can demonstrate reasonable matches to empirical profiles using time-averaged properties [21, 22, 27, 28]. It can be shown, however, that when these approaches are implemented self-consistently into a simulation, the outputs of these models can deviate markedly from experimental measurement, often resulting in overly relaxed plasma properties and transport profiles[29, 31].

With that said, our recent experimental work has suggested that the key premise that has guided these previous efforts, that the collision frequency is highly non-linear, may not be valid. Specifically, a new application of non-invasive laser diagnostics has allowed direct measurements of the anomalous collision frequency. We have found from these profiles that the actual collision frequency varies by only two orders of magnitude on the length scale of the thruster [32, 33]. This type of relaxed profile still yields strongly peaked electric fields because we have also found that the electron temperatures in the discharge are nearly twice as large as previously expected [33, 34]. The higher electron temperatures produces a stronger electron pressure gradient, which, when combined with the generalized Ohm's law, allows for larger electric fields without the need for orders of magnitude variation in the collision frequency [34].

The finding that the anomalous collision frequency may exhibit less variation invites the re-consideration of closure models that previously had been dismissed. Before undertaking this investigation, however, it is necessary to also incorporate the necessary physics to allow the models to self-consistently capture the higher electron temperatures in the model. To this end, in a follow on investigation to our experimental measurements of the collision frequency, we sought to explain why the electron temperatures might be higher in the discharge than previously predicted with model results. Our key finding was that the typically form of electron heat flux and wall losses that are used in fluid simulations may be overpredicting the energy transport and amount of energy lost to walls [35]. We showed that by modifying these terms in the electron energy equation, we were able to recover the high electron temperatures in the discharge. At the same time, our companion paper (Ref. [36]) found that neglecting the electron heat flux along field lines qualitatively captured the recently observed fact that magnetic field lines in these devices may be non-isothermal [36–38]. We in turn showed that the steep electric temperatures allowed for substantially more relaxed spatial variation of the anomalous collision frequency.

This previous work has the major caveat that it was based on employing our experimentally-measured collision frequency profile in the model while we parametrically varied the electron thermal conductivity and flux to the thruster walls. We have yet to explore self-consistently any closure models with this modified heat flux. In light of the promising impact heat flux may have on the efficacy of the closure models, the need is thus apparent for a parametric investigation of a self-consistent transport profile with modifications to the heat flux. To this end, the rest of this paper is organized as follows. In section III, we review a Hall thruster operation and the multi-fluid framework to Hall thruster modeling. In section IV, we outline our self-consistent closure model and modifications to the electron heat flux and wall losses. In section V we describe the multi-fluid model used in this work, along with details of the numerical implementation of our models. In section VI, we present global, one-dimensional, and two-dimensional results of the closure model using different forms of the heat flux and wall loss coefficients. Section VII varies the collision frequency coefficient values, and explores extensibility across operating conditions. Finally, in section VIII we discuss the performance of the model and the potential for heat flux modifications to enable first-principles closures.

III. Hall thruster fluid modeling

In this section, we first describe the principle of operation and geometry of a typical Hall thruster. We then review a standard multi-fluid treatment of the plasma in this device.

A. Hall thruster principle of operation

Figure 1 displays a Hall effect thruster and notional simulation domain in axial-radial coordinates. A Hall thruster consists of four main components: a cathode, anode, discharge chamber, and magnetic circuit. For operation, a potential

difference is established between the anode and cathode. This potential attracts the electrons emitted by the cathode towards the anode. As the electrons enter the discharge channel, they are confined by a mostly radial magnetic field established by the magnetic circuit. Along centerline, the magnetic field typically peaks near the channel exit. The combination of this magnetic field with the axially pointing electric field creates an $E \times B$ drift in the azimuthal direction that confines the electrons. Neutral gas is then injected at the anode and is ionized when it encounters this trapped electron population. The electrons stripped from the neutrals replenish this population as electrons migrate towards the anode through these collisions. The ions are then accelerated out of the device by the electric field, producing thrust. This ion population is followed by new electrons emitted by the cathode, which ensures the plasma remains quasi-neutral throughout the device.

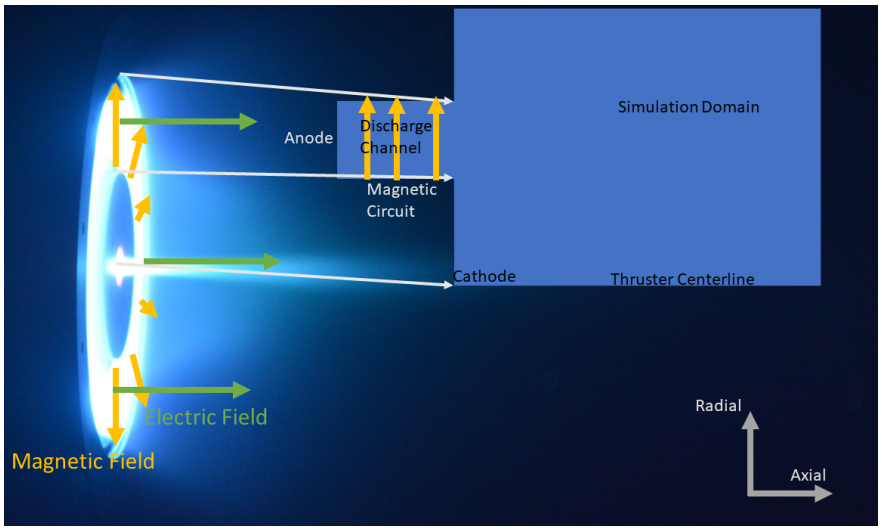

Fig. 1 Operating Hall thruster with notional simulation domain. Note the axial-radial coordinate frame in the lower right.

Figure 2 displays a typical distribution of plasma properties along the channel centerline of a thruster. For conciseness, we use the following abbreviations: n_e is the electron number density, T_e is the electron temperature, and E_z is the axial electric field. The axial electric field exhibits a steep peak near the exit plane near the location of the peak magnetic field. The electron motion across field lines is highly impeded here, giving rise to the enhanced electric field. This concentrated field in turn promotes greater Ohmic heating, leading to the peaked electron temperature profile. The heated population has sufficient energy to ionize inflowing neutral gas which increases the number of electrons in the exit plane region. As these electrons traverse from the downstream region toward the anode, the density becomes self-reinforcing as the large electron density maintains the ionization rate, even as the temperature cools in the channel.

B. Review of multi-fluid approach to Hall thruster modeling

In this section, we first outline the multi-fluid equations to the ions. We then detail the particle and momentum transport of electrons. We conclude with a description of the bulk electron energy transport.

1. Ion dynamics

In a multi-fluid approach to Hall thrusters, the ion dynamics are captured by two main equations: continuity, and momentum. The continuity equation is given by [6]

$$\frac{dn_i}{dt} + \nabla \cdot (n_i \vec{v}_i) = \dot{n}, \tag{1}$$

where n_i is the ion number density, $\vec{v}_i$ is the ion velocity, and $\dot{n}$ is the ionization source term. Physically, the time rate of change of the ion density is balanced by flux and a production term. For the ion momentum, the ions are considered

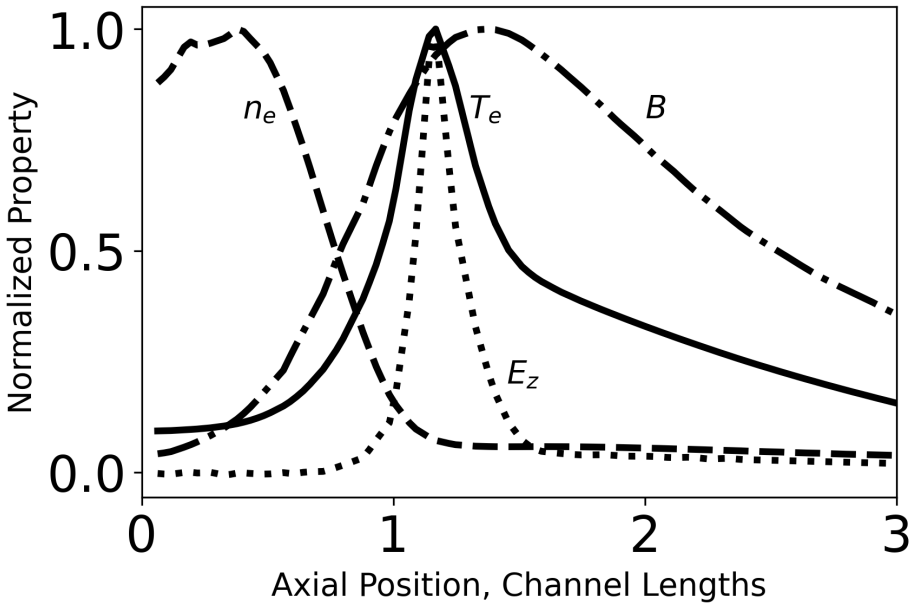

Fig. 2 Normalized electron properties as a function of axial position.

to be unmagnetized due to their large mass. This assumption results in the governing equation [6]

$$m_i n_i \frac{d\vec{v}_i}{dt} + m_i \nabla \cdot (n_i \vec{v}_i \vec{v}_i) = q_i n_i \vec{E} - \nabla P_i + R_i, \tag{2}$$

where q_i is the ion charge, $\vec{E}$ is the electric field, P_i is the ion pressure, and R_i is the net force on the ions due to collisions with other species. Physically, this relationship captures the fact that the time rate of change of bulk ion momentum is equal to a flux and source contributions from the electric field, pressure forces, and collisional forces. While some models [6, 39] close the system of equations by treating the ions as isothermal, it is also possible to include an energy equation which is then closed with a Spitzer-Harm like heat flux [40]. To account for ion populations with different bulk velocities, it is possible to solve the set of transport equations for each ion population, which is where the name "multi-fluid" arises.

2. Electron continuity and momentum

When treating the electrons in Hall thrusters, fluid models typically make a number of approximations to simplify the system of equations. The first assumption is quasi-neutrality:

$$n_e = \Sigma_Z Z n_{i,Z}, \tag{3}$$

where n_e is the electron density, Z is the charge state of the ions and $n_{i,Z}$ is the number density of ions of charge state Z. For a full fluid representation, the ion density comes from Eq. 3, removing the need to solve an electron continuity equation. To capture the electron momentum transport, the electrons are treated as inertialess, which results in the generalized Ohm's Law:

$$\vec{j}_e = \frac{e}{m_e \nu_e} \left(\nabla P_e + e n_e \vec{E} - \vec{j}_e \times \vec{B} - \frac{m_e \nu_{ei}}{e^2 n_e} \vec{j}_i \right), \tag{4}$$

where $\vec{j}_e$ is the electron current density, e is the fundamental charge, m_e is the electron mass, ν_e is the total electron collision frequency P_e is the electron pressure, $\vec{B}$ is the magnetic field, ν_{ei} is the electron-ion collision frequency, and $\vec{j}_i$ is the ion current density. Typically, the magnetic field is a stationary profile that is treated as a model input while the electric field can be solved by combining Ohm's law with current continuity [6]. Physically, Eq. 4 demonstrates that the electrons can be accelerated by thermal expansion or an electric field, magnetic fields confine the electrons, and there is

an effective drag force between the ions and electrons. Numerically, the neglect of electron inertia and the electron continuity equation removes the need to explicitly evaluate an electron flux, which reduces computational complexity and allows for larger timesteps.

The electron collision frequency in Eq. 4 has five contributions:

$$\nu_e = \nu_{ei} + \nu_{en} + \nu_{iz} + \nu_w + \nu_{an}, \tag{5}$$

where ν_{en} is the electron-neutral scattering collision frequency, ν_{iz} is the ionization frequency, ν_w is the electron-wall collision frequency, and ν_{an} is the anomalous collision frequency. The first four terms combined represent the classical collision frequency effects and have generally accepted representations based on classical theory. These include forms for the electron-ion [41] and wall [20] collisions as well as cross sectional forms for the scattering and ionization collisions [42]. The anomalous collision frequency does not have a first-principles form, as mentioned in Sec. II, but will be discussed in subsequent sections.

3. Electron energy

The electron energy transport we employ is for the internal energy form, i.e. the evolution for the electron temperature[6]:

$$\frac{3}{2} e n_e \frac{\partial T_e}{\partial t} + \nabla \cdot \left(-\frac{5}{2} \vec{j}_e T_e \vec{v}_e + \vec{q} \right) = \vec{E} \cdot \vec{j}_e + Q - \frac{3}{2} T_e \nabla \cdot \vec{j}_e, \tag{6}$$

where T_e is the electron temperature, $\vec{q}$ is the electron heat flux, and Q is a source term that represents energy losses due to collisions. Physically, the left hand side consists of a time rate of change and two flux terms: a convective flux and heat flux. The right hand side captures energy sources which, from left to right, consist of Ohmic heating, collisional losses, and an additional term that arises from pulling the number density out of the time derivative. Classically, the heat flux is treated with a Spitzer-Harm form that depends on the collisions and gradients in temperature. We have shown in recent work, however, that this may not be a valid representation and may require modification [36]. We revisit this issue in the following section.

IV. Proposed closure models for momentum and heat flux

In this section we first describe the first-principles anomalous collision frequency closure we employ in this work. We then discuss the forms of the heat flux we will utilize in our investigation. Finally, we detail the scaling of the electron energy losses to the walls that is utilized to match higher electron temperatures.

A. Collision frequency model

As discussed in Sec. II, and shown from previous work [17, 29], the most critical feature for an anomalous transport model is to have a minimum near the location of peak magnetic field. Physically, this feature reduces the ability for electrons to cross magnetic field lines and thereby promotes a sharply peaked electric field. Historically, this type of minimum has been accomplished by employing a semi-empirical form for the anomalous collision frequency based on a Bohm-like formulation:

$$\nu_{an} = \beta(z)\omega_{ce}, \tag{7}$$

where β is a coefficient that spatially varies as a function of axial position z. Figure 3 shows one such profile from a previously calibrated Hall thruster simulation [30].

While this type of profile has previously yielded simulations that match several quantities of interest, recent experimental measurements performed in a Hall thruster have indicated that the actual transport may differ. To this point, we show in Fig. 3 for the same operating condition and thruster the actual measured anomalous collision frequency profile for comparison [34]. The most notable contrast between the two profiles is that the measured closure only varies by two orders of magnitude while the empirically-inferred closure varies over almost three orders of magnitude. As we discussed in Ref. [34], this disparity can in large part be attributed to the high electron temperatures in the experimental discharge.

In light of the fact that the actual collision frequency profile may be more relaxed, we consider in this work as an exploratory study a highly simplified, first principles-inspired closure: an augmented form of the classical electron-ion

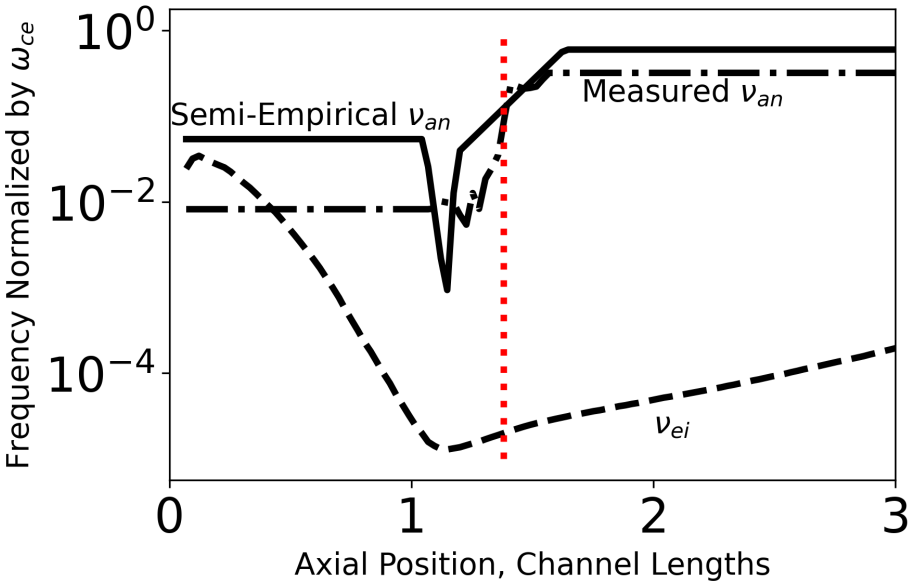

Fig. 3 Representative Bohm-like coefficient as a function of axial distance from the anode for operation on krypton at 300V 15A. Distances have been normalized by the channel length. The dashed red vertical line denotes the location of peak magnetic field.

collision frequency:

$$\nu_{an} = 2.9 \times 10^{-12} c \frac{n_e ln(\Lambda)}{T_e^{\frac{3}{2}}}, \tag{8}$$

where c is the scaling coefficient and $ln(\Lambda)$ is the Coulomb logarithm. For this work, the Coulomb logarithm is calculated as a function of n_e, T_e, and the effective ion charge [41]. Physically, the inverse dependence on the electron temperature allows for a minimum, which is necessary to provide a transport barrier promoting an enhanced electric field. However, Fig. 3 shows how the ν_{ei} profile has a broader and shallower local minimum. We therefore anticipate this profile will be more relaxed overall.

B. Heat flux model

Classically, the heat flux in Eq. 6 is represented with a Spitzer-Harm [40] form

$$\vec{q} = -\kappa \nabla T_e \tag{9}$$

where κ is the thermal conductivity. For magnetized electrons, such as in a Hall thruster, the form of the conductivity depends on the direction relative to the magnetic field [43]

$$\kappa_{\parallel} = a(Z^*) \frac{n_e T_e}{m_e \nu_{e,c}} \qquad \kappa_{\perp} = b(Z^*) \frac{n_e T_e \nu_e}{m_e \omega_{ce}^2}, \tag{10}$$

where $\parallel$ and $\perp$ indicate the parallel and perpendicular direction to the magnetic field, $\nu_{e,c}$ is the classical electron collision frequency, a and b are coefficients based on the effective charge state Z^*, and ω_{ce} is the electron cyclotron frequency. Physically, collisions reduce conductivity along field lines while enhancing conductivity across them and the cyclotron term in the perpendicular conductivity accounts for the confinement of the electrons. In Hall thrusters, the anomalous collision frequency is generally thought to only act in the perpendicular direction, hence why only classical collisions are included in the parallel conductivity.

The validity of this classical formulation of the heat flux parallel to field lines implicitly rests on the assumption that the plasma is collisional. In practice however, the mean free path of electrons along magnetic field lines in the thruster is such that the high-energy tails of the distribution are effectively collisionless [36]. Per the Spitzer-Harm conductivity in

Eq. 10, this low collisionality would cause the conductivity along magnetic field lines to become unphysically large. This behavior introduces the possibility that this conventional representation of the heat flux is not valid.

To help address this issue, related sub-fields of plasma physics such as solar wind and laser plasma models have adopted free-streaming heat flux limiters [44]. These limiters have a free-stream limit that sets the heat flux equal to a convective-like form [44] multiplied by a scaling parameter α

$$\vec{q} = \alpha e n_e T_e \vec{v}, \tag{11}$$

where $\vec{q}$ is the heat flux and $\vec{v}$ is a velocity. However, the exact form of these limiters varies, particularly in the form of the velocity. Some investigators have opted for the thermal velocity [45] while others recommend the average bulk velocity [46]. As such, we explore a set of alternative forms for replacing the parallel heat flux in our model, which are detailed in the following subsections.

We note here that for all cases, we only apply the free-stream heat flux in the parallel direction, with the perpendicular heat flux following the Spitzer-Harm form. The only deviation from Eq. 10 is that we do not include the anomalous collision frequency in the perpendicular conductivity. Our previous work showed that doing so would artificially lower the electron temperature [35].

1. Convective Bulk (CvB)

The first form we consider uses the bulk electron velocity as the velocity in Eq. 11. This form appears to have been proposed first in the context of modeling the solar wind [44, 46, 47]:

$$q_{\parallel} = \alpha e n_e T_e v_{e,\parallel}, \tag{12}$$

where the subscript $\parallel$ indicates that we are applying the free-stream heat flux only in the direction parallel to the magnetic field. Here, the electron heat flux is convected in the same direction as the bulk velocity with the same magnitude. For brevity, in the rest of this work, we will refer to this as the "CvB" form of the heat flux.

2. Convective Thermal (CvTh)

The second form of the heat flux uses the electron thermal velocity as the heat flux convective velocity. As with the CvB version, the motivation primarily comes from previous use [45], although this form is not as popular as the convective bulk case. Additionally, as finite volume computational fluid dynamics requires a direction to evaluate fluxes across cell boundaries, when evaluating the heat flux, we assume the heat flux remains in the direction of the bulk velocity. Formally, this version is

$$q_{\parallel} = \alpha e n_e T_e v_{e,th} \hat{v}_{e\parallel}, \tag{13}$$

where $v_{e,th} = \sqrt{\frac{2eT_e}{m_e}}$ is the thermal velocity and $\hat{v_{e\parallel}}$ is a unit vector pointing in the direction of the bulk electron velocity for the purposes of calculating flux across a cell edge. Physically, this form transports energy in the same direction as the bulk velocity but at the thermal velocity magnitude, which is typically higher in Hall thrusters. For the remainder of this paper we refer to this form as "CvTh."

3. Convective Flux (CvFlux)

The final form of the heat flux we consider builds upon the use of the thermal velocity but does not assume it convects in the direction of the bulk velocity. Rather, it is assumed that electrons free-stream across the boundary between cells and the net effect is the relative difference between the flux leaving each cell. In terms of two neighboring cells, this flux is

$$q_{\parallel} = \alpha e((n_e T_e v_{e,th})_{cell1} - (n_e T_e v_{e,th})_{cell2}). \tag{14}$$

Physically, this form allows for electron energy to be transported from regions of high energy to regions of low energy. In other words, the directionality of this form is not fixed to the direction of the bulk velocity, allowing energy to travel against the direction of the bulk electron flow. We denote this form "CvFlux" for the rest of this work.

C. Wall loss modification

In addition to the heat flux modifications, we employ a modification to the electron energy losses to the thruster walls. There are three motivations for our use of this scaling. First, thermal modeling of Hall thrusters has previously lowered

the plasma loading to the walls to match observed temperatures[48]. Second, for magnetically shielded thrusters, effects like magnetized sheaths and magnetic mirrors may become important and serve to reduce the electron flux to the walls [35, 49]. Third, in our previous modeling work, we found that in order to match experimentally- observed temperatures, reducing wall losses would bring simulation properties more in line with measurement [35].

Following this previous work, we introduce a global scaling factor in front of the electron flux into the thin sheath formed at the walls

$$\vec{j_e} \cdot \hat{n} = c_w j_{e,th} e^{\frac{max(\Delta\phi,0)}{T_e}}, \tag{15}$$

where $\vec{j_e}$ is the electron current density $\hat{n}$ is the normal vector pointing into the wall, c_w is the tunable wall loss scaling coefficient, and $\Delta\phi$ is the potential drop across the sheath. Physically, this form follows the typical electron flux into the sheath but with the added ability to tune its magnitude to match experimental results.

V. Numerical implementation

In this section we first describe the multi-fluid model utilized in this work. We then detail numerical implementations we made to ensure stability of the simulations with the closures outlined in Sec. IV. Finally, we describe the thruster, operating conditions, and experimental dataset we employed for validation and calibration.

A. Model overview

We employed in this work Hall2De, a 2D axisymmetric axial-radial model developed by the Jet Propulsion Laboratory. As the code has been extensively described elsewhere [6, 50, 51] we confine our discussion here a high-level description. The electron current density, temperature, and the electrostatic potential are solved along a magnetic-field aligned mesh (MFAM) while the electron number density is handled via a quasi-neutrality assumption. The generalized Ohm's law is combined with current conservation to first solve for the potential, which is then used to solve for the current density.

The electron boundary conditions require the potential to be specified at the anode and cathode and the temperature to be specified at the cathode and far-field boundaries. For numerical stability, the electron solver may take a smaller timestep than the heavy species, which is at most a factor of five lower. Heavy species are solved on an axial-radial (z-r) mesh, as they are not considered magnetized.

The neutrals are solved using a viewfactor algorithm that treats them as free-streaming from emitting surfaces until they are either ionized, reflected at the walls, or leave the domain [50]. The ions are treated as a fluid and the continuity, momentum, and energy equations are solved. Due to the existence of distinct ion populations, such as ions born in the channel and at the cathode [52], Hall2De allows for multiple ion fluids. The fluids are distinguished by the value of the electrostatic potential in the cell they are born in.

Table 1 describes the model free parameters employed in this work. We used two ion fluid populations with ions born at or above 240V assigned to the beam population and those below assigned to the cathode population. The cathode input properties are based on standalone measurements of cathode properties [53] and the 2.5 eV far-field temperature is in the middle of the typical range for Hall thrusters [6]. The timestep was set at the highest possible stable value. We simulated for a total of 1.5 ms. The results presented in the following represent time-averages of all the plasma quantities of interest over that simulation duration.

B. Numerical implementation of modified closures

Self-consistent implementations of anomalous collision frequency closures are known to introduce numerical instability in simulations [54]. To avoid this issue, we apply a relaxation factor to the update of the anomalous collision frequency

$$\nu_{an} = r\nu_{an,new} + (1 - r)\nu_{an,old}, \tag{16}$$

where r is the relaxation factor, $\nu_{an,new}$ is the value from Eq. 8 using the plasma properties from the current timestep, and $\nu_{an,old}$ is the value using the plasma properties from the previous timestep. Numerically, this factor dampens large transients that may drive the simulation unstable. In this work, we employ a value of 0.5 as that was empirically found to be the largest value that maintained consistent stability.

In addition to the relaxation factor, we note here that the anomalous collision frequency is calculated at every edge on the MFAM except boundary edges. The determination of the collision frequency based on the local plasma properties everywhere in the domain is in contrast to previous approach empirical closures. In these approaches, it is common

Table 1 Hall2De Simulation Parameters

Parameter	Value
Number of ion fluids	2
Discriminating Potential	240 V
Maximum charge state	3
Cathode flow fraction	7 %
Cathode ionization fraction	5 %
Cathode electron temperature	3.0 eV
Cathode potential	0 V
Far field electron temperature	2.5 eV
Wall material	Boron Nitride
Wall temperature	500 °C
Heavy Species Timestep	15 ns
Simulation duration	1.5 ms
Collision frequency relaxation factor	0.5

to only specify the value of the collision frequency along centerline. These values are then extrapolated along field lines–typically with a scaling factor to capture the impact of the magnitude of magnetic field[17].

For the heat flux, the primary numerical factors are the directionality and semi-implicit treatment of the electron energy equation. To apply the free-stream heat flux in the parallel direction only, we take advantage of the fact that electrons are solved along a MFAM, which already distinguishes between the parallel and perpendicular directions. In Hall2De, the electron energy equation is handled semi-implicitly [6]. Generally, the convection and heat flux terms are treated implicitly while the thermal conductivity and any source terms are handled explicitly. For the CvB and CvTh cases, this implementation remains valid as they effectively serve to adjust the coefficient in front of the convective flux. The CvTh case uses a similar explicit implementation as the thermal conductivity, as current temperature is used in determining the thermal velocity. However, we implement the CvFlux case explicitly such that the net energy is added to the cell with the lower thermal flux and removed from the cell with the higher thermal flux.

C. Simulated test article and operating conditions

We modeled in this work the H9 thruster, a 9 kW class magnetically-shielded Hall thruster jointly developed by the University of Michigan, Jet Propulsion Laboratory, and the Air Force Research Laboratory [55]. Figure 1 displays the H9 in operation on the left hand side. Table 2 lists the operating conditions we considered in this work. For each of these conditions, we have experimental measurements of ion velocity along centerline, electron number density and temperature, and axial electric field [36].

These data were all measured using the non-invasive laser diagnostics of laser-induced fluorescence (LIF) to probe the ion properties and electric field and incoherent Thompson scattering for the electron properties [36]. We note here that most of our analysis focuses on the krypton 300V 15A condition, as it has 2D measurements of the electron temperature and number density along a magnetic field line in addition to the centerline properties [36].

Table 2 H9 Operating Conditions

Parameter	Value
Propellants	krypton, xenon
Discharge Voltage	300V, 600V
Discharge Current	15A, 30A

VI. Results: comparison of heat flux closure models

We present in this section the results of the self-consistent implementation of the modified form of the electron-ion collision frequency and the three forms of the heat flux closure. We first show trends in the plasma properties as a function of axial position along centerline. We then compare the simulated and experimental thruster performance metrics. We conclude by examining the effects of these flux closures on the two dimensional electron properties along a magnetic field line.

A. Effect of alternative heat flux formulations on plasma properties on channel centerline

We show in Fig. 4 the simulation result and experimental measurement of the a) ion velocity, b) electron temperature, c) electron density, and d) electron collision frequency as a function of position along channel. The coordinates in these results are referenced with respect to the anode position and normalized by channel length. For all these figures, we assumed a common scaling coefficient for the effective collision frequency (Eq.8) with $c = 1000$. This value was chosen based on Fig. 3 where we can see the local minimum of the ν_{ei} is approximately three orders of magnitude lower than the calibrated ν_{an} value. We then parametrically varied the values of the scaling factor for the heat flux, α, and the wall loss factor, c_w. We show in the plot the results for each flux model with the coefficients that exhibited the best qualitative agreement with the experimental measurements of ion velocity. This is one of the most common metrics that is employed for model calibration [17].

We adopt the abbreviations for the heat flux methods defined in Sec.IV as well as "SH" for the Spitzer-Harm heat flux. Additionally, we display two wall loss cases for the SH flux: one with $c_w = 1$ and one with SH $c_w = 0.01$. By comparing these two SH cases, we can observe the effect of varying the wall loss coefficient only, which allows us to separate out the impact of adjusting the wall loss coefficient from adjusting the heat flux.

1. Ion velocity comparison

As can be seen from Fig. 4 a), all formulations of the heat flux cases exhibit qualitative agreement with the experimental profile for ion velocity. The CvB and CvTh are slightly closer to the knee in the ion velocity profile at z=1.0. This difference indicates that these cases have a larger electric field magnitude, which is in closer agreement with the data

The most significant discrepancy between the flux forms is within the channel. Unfortunately, we cannot make a quantitative comparison here due to the lack of experimental data in this region. However, we do note that it is typically thought that the potential inside the channel is approximately constant [17]. As the electric field represents the gradient of the potential, we therefore expect the ion velocity profile inside the channel to be relatively flat, with the exception of the region near the anode. We therefore consider the cases with $c_w < 1$ to better capture the thruster dynamics as the SH $c_w = 1$ case has significant ion acceleration in the channel. Qualitatively, this result suggests that reduced wall losses are a contributing factor to maintaining low electric fields in the channel.

2. Electron temperature comparison

We show in Fig. 4 b) the electron temperature profiles as a function of axial distance from anode. We can see that for all the closures, reducing the wall loss coefficient, c_w, results in higher peaked electron temperatures. This is physically intuitive–with a reduced energy sink from the plasma, higher internal energies can be supported. With that said, even the best case closures (CvB and CvTh) exhibit peak electron temperatures that are ~ 15 eV below the measured peak. Physically, this suggests that these models overestimate heat flux out of the thruster geometry. Intuitively, the two models that inherently have lower heat flux—CvB and CvTh— provide marginally higher temperatures (by approximately 4 eV).

3. Electron density comparison

Figure 4 c) displays the variation along channel centerline of the electron number density for varying flux closures and wall loss coefficients. As with the ion velocity curve, most of the methods closely match the experimental data in the region where it is available but differ in the channel. This close match to the number density is unexpected as the electron temperatures are lower than the peak experimentally-observed (Fig. 4 b) temperature. This latter result would imply we should be under predicting the ionization rate and thus the number density. This discrepancy may in part be explained by the slower simulated ion velocity profile near the channel exit, as it indicates the plasma is not fluxing with as high of a speed. The lower speed requires a higher number density before the flux leaving the region balances the source term. In this manner, it is possible to match the number density with a lower ionization rate.

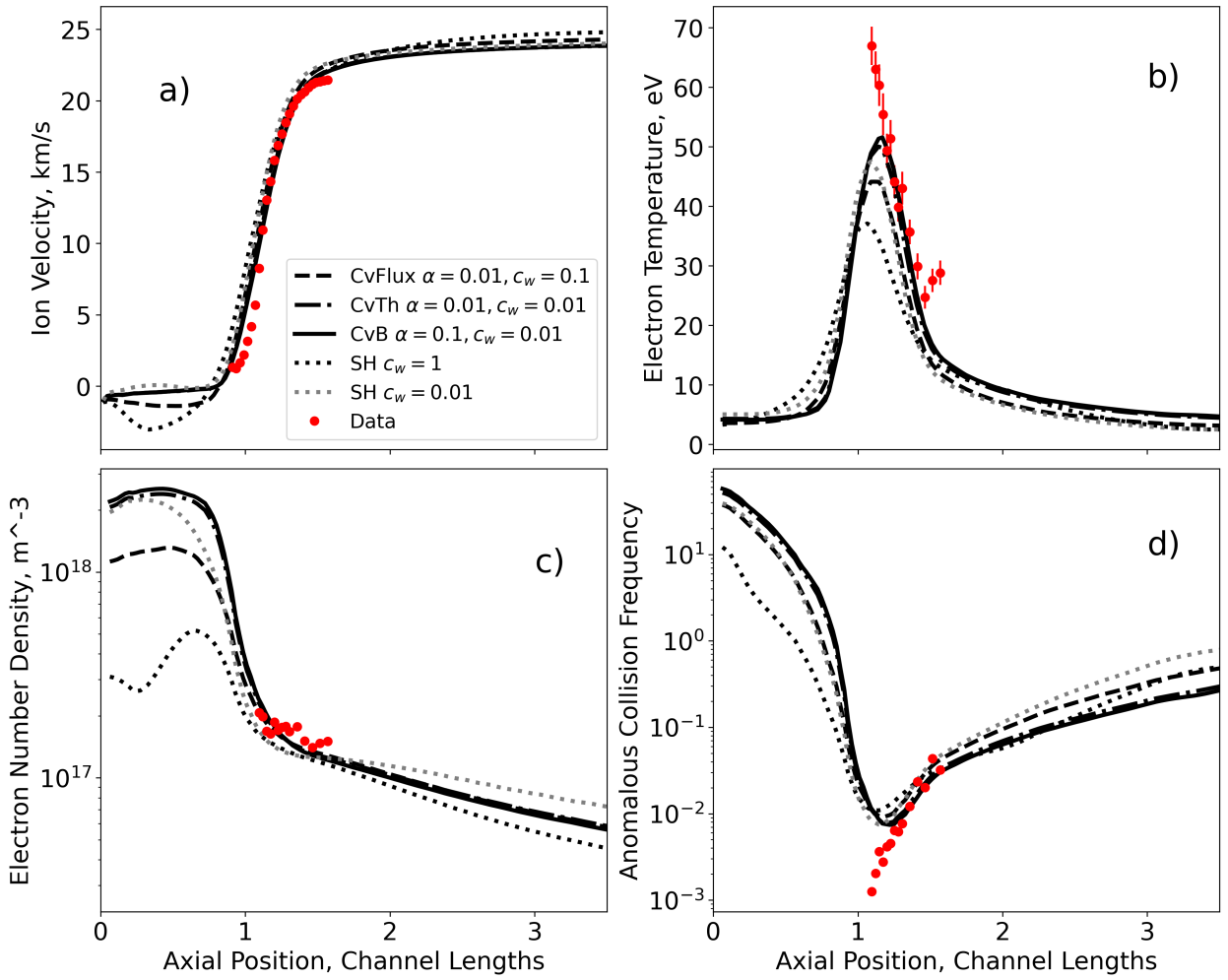

Fig. 4 Plasma properties along channel centerline for alternative forms of the electron heat flux with c=1000. The thruster was operating on krypton at 300V and 15A. a) shows the ion velocity profile, b) the electron temperature profile, c) the electron number density profile, and d) the anomalous collision frequency profile normalized by the cyclotron frequency.

4. Collision frequency comparison

Fig. 4 d) shows the simulated collision frequency along with the experimental profile from Ref. [36]. As can be seen, all the results exhibit similar behavior: the model results match the data at $z \sim 1.5$ channel lengths but exhibit a shallower local minimum. The higher collision frequency for all the cases near the channel may in part explain why the ion velocity profiles in this region are not as steep as shown in the experiential data (Fig. 4 a). A higher collision frequency allows for more cross-field electron current and therefore requires a lower electric field. This field will translate to less rapid ion acceleration.

We note here that he higher local minimum is in large part directly caused by the fact that we do not capture the same peak temperatures in the computational results. As the collision frequency closure is inversely dependent upon the electron temperature, larger peak temperatures would increase the magnitude of the dip near the channel exit.

B. Effect of free-stream heat flux on global performance metrics

Fig. 5 plots the performance metrics of discharge current, thrust, and anode efficiency normalized by their experimental values. In all cases, the global metrics are under predicted. However, the CvB and CvTh and SH case with higher wall losses exhibit improved agreement when compared to the more standard SH $c_w = 1$ case. The dominant

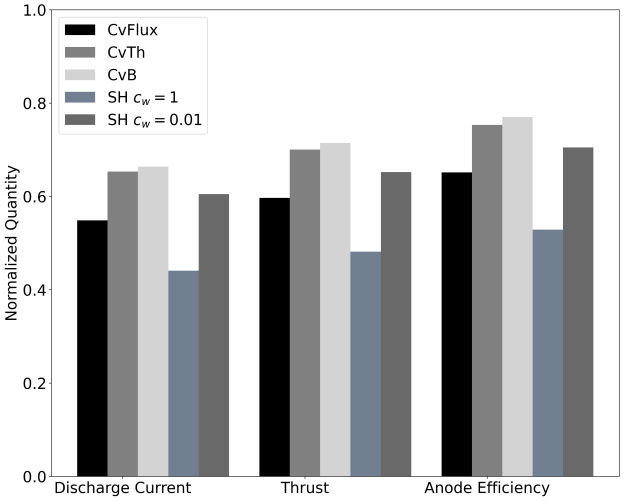

Fig. 5 Global performance metrics for alternative forms of the electron heat flux with c=1000. The thruster was operating on krypton at 300V and 15A. Note that each quantity is normalized by its experimental value. Experimental values are from Ref. [56]

driver of the poor match for the best case, CvTh, with global metrics is the simulated mass efficiency, which indicates the degree of ionization, as it is approximately 15% lower than the experimental value. This may in part be explained the peak temperatures are lower than experimentally shown (Fig. 4 b), which would underpredict the ionization rate.

C. Effect of free-stream heat flux on plasma properties off centerline

We show in Figure 6 plots of the electron temperature and density as a function of radial position along a fixed magnetic field in the thruster. This field line intercepts the thruster centerline at approximately the location of peak magnetic field. As can be seen from the electron temperature results, the Spitzer-Harm formulation results in an isothermal field line at a temperature of 18.2 eV. This finding is to be expected, as the high thermal conductivity along field lines with this model allows them to isothermalize quickly. Indeed, as has been exhibited extensively in previous modeling efforts that baseline a SH approach, the field lines in the thruster are isothermal [10, 18, 57].

In contrast, we see that both the CvB and CvTh closure cases match the data within error bars. There is an unusual feature–a dip near channel centerline–for the CvB case, though we suspect it is a meshing artifact. This small feature notwithstanding, the quantitative agreement of these closures with the experimental data in two dimensions provides compelling evidence that the heat flux in the parallel direction is more nuanced than classical SH formulation.

Turning to the plasma density, we see that all the flux closures provide a profile qualitatively similar to the experimental data and characterized by a peak on centerline with a drop as the field lines approach the edges of the channel. In contrast to the electron temperature profiles, however, the simulated number density only matches the magnitude of the experimentally-measured density on the side of the channel closest to thruster centerline. The reasons for the disagreement at the larger radii can be explained by a breakdown in quasineutrality due to low number densities making the Debye length comparable to cell size in the region of the outer front pole [58]. While recent versions of Hall2De correct for this behavior [58], we did not employ these adjustments in this work. With that said, we do note that this field line is located at z=1.4 on centerline, which is where the model for our collision frequency (Fig. 4 c) begins to exhibit a departure from simulation. This discrepancy may be correlated with the observed two-dimensional behavior.

D. Summary

In this section we presented comparisons to global, one-dimensional, and two-dimensional measurements for each heat flux closure. We find that all closures qualitatively capture the spatial distribution of the local plasma properties along centerline but exhibit quantitative discrepancies. In particular, the peak electron temperature is under predicted by 25% by the best-case heat fluxes. This result translates to a lower ionization rate, which in turn leads the global performance metrics (which are directly tied to the degree of ionization) to be lower than in the experiment. The closures differ most in the behavior along field lines in two dimensions, with only the CvTh and CvB forms of the heat flux able

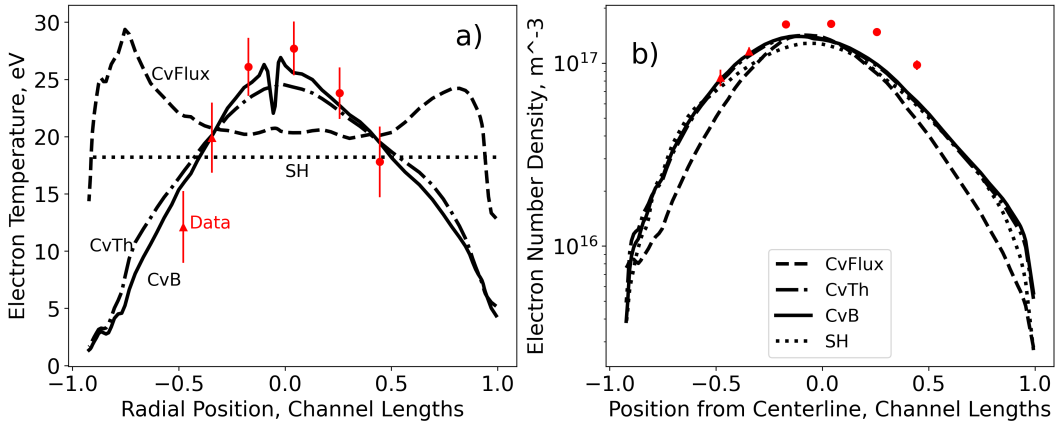

Fig. 6 a) Electron temperature and b) density along magnetic field line for various forms of the parallel electron heat flux. The points denote experimental measurements. The axial position of this field line at centerline is 1.4 channel lengths. The coefficients for all free-stream models is the same as Fig. 4 while the Spitzer-Harm flux uses $c_w = 0.01$.

to capture two-dimensional variation in plasma properties along a field line. Based on the whole of our results, we ultimately conclude the CvTh is the best case heat flux. We subsequently baseline this heat flux model in the following section and investigate parametrically the effect of adjusting the scaling coefficient of the anomalous collision frequency.

VII. Results: evaluation of collision frequency model

Armed with the results from the previous section, we parametrically evaluate here the "best" heat flux closure model, the CvTh free-streaming heat flux model with the best-model parameters, $\alpha = 0.01$ and $c_w = 0.01$. We first evaluate the impact of varying the anomalous collision frequency scaling coefficient on the centerline properties. We then consider the extensibility of the closure models to different operating conditions.

A. Effect of anomalous collision frequency coefficient

We examine in this section the effect of tuning the scaling coefficient c in Eq. 8. To this end, Fig. 7 shows the ion velocity and electron temperature along channel centerline for various values of the coefficient. From this graph, we see that as c increases, ion velocity profile moves further downstream and becomes more spatially relaxed. Physically, this result is due to a relaxing electric field. Per the generalized Ohm's law (Eq. 4), the electric field magnitude scales inversely with the collision frequency. Thus, when the scaling factor is sufficiently high, the minimum value of the collision frequency profile is insufficiently small to locally impede cross-field electron motion resulting in a lower electric field. As a secondary effect, the lower electric field that results from lower c values also yields ions with a lower ultimate velocity. Overall, we see that the value of c=1000 provides the best match over the range of available data.

Figure 7 b) shows the electron temperature profile as a function of the scaling coefficient c. It exhibits a similar downstream shift with increasing c to the trend exhibited by the ion velocity profile in Fig. 7 a). We also observe that the peak electron temperature continues to increase with the scaling coefficient until $c > 2000$ where the peak temperature subsequently decreases at $c = 5000$. The initial rise with c is notable because, as we remarked previously, the electric field magnitude lowers with c. We therefore might expect the peak temperature to decrease since Ohmic heating scales with electric field[29]. As a mitigating factor, however, we note that increased c also can promote more cross-field current, which will enhance Ohmic heating. The interplay between these two effects ultimately may contribute to the fact that the peak temperature is non-monotonic with c.

Fig. 8 shows the predicted discharge current as a function of the scaling coefficient. The increase we see is likely driven primarily by the increase in cross-field mobility. Notably, all values of c underpredict the discharge current, but $c = 5000$ is within 5% of the observed value. With that said, as Figure 7 exhibits, we find that $c = 5000$ exhibits arguably the worst agreement with the centerline profiles. In practice, the fact that there is a not a singular coefficient that yields agreement with both global and local plasma properties points to a possible deficiency of the model. We return to this point in Sec. VIII.

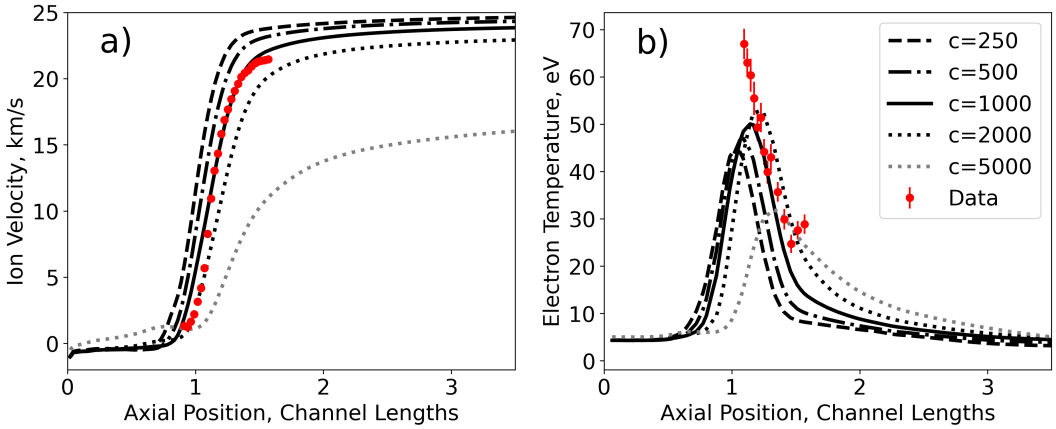

Fig. 7 a) Ion velocity and b) electron temperature along channel centerline for different values of the anomalous collision frequency scaling coefficient. All cases employ the CvTh model for parallel heat flux.

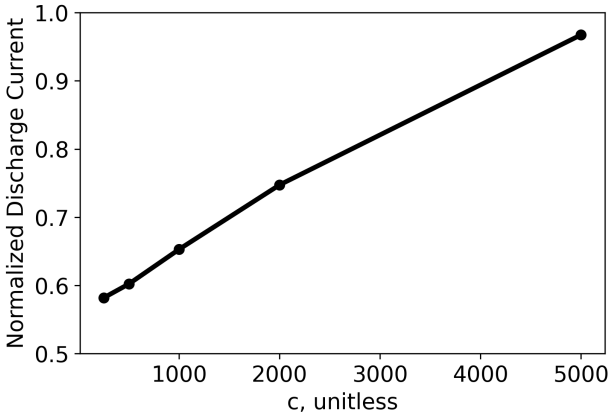

Fig. 8 Discharge Current as a function of the coefficient for anomalous collision frequency. All cases employ the CvTh model for parallel heat flux.

B. Extensibility to other operating conditions

While the above sections have shown that the self-consistent model can be tuned to match several plasma and global properties, this analysis was confined to a single operating condition– 300 V and 15 A with krypton propellant. In this section, we explore the extensibility of this model to the other operating conditions outlined in Table 2. In each case, we tune the scaling coefficient in Eq. 8 but hold the energy transport parameters constant with a CvTh free-stream flux with $\alpha = 0.01$ and a wall loss coefficient of $c_w = 0.01$. The metric we used for adjusting the parameter is the agreement with the centerline ion velocity profile measurements.

Figure 9 displays the ion velocity profiles for each case compared to experimental LIF data. As can be seen, in all cases, the simulated ion profile can be made to match the experimental data in both location and magnitude. This highlights the extensibility of the model subject to only one variable parameter, c. We caveat this result with the fact that the dependence on this free parameter–while more efficient than some previous approaches to model calibration–still means the model is not fully predictive. With that said, it is possible that the variation in c we see across the operating conditions exhibited in Fig. 9 could provide clues to help address this failing by informing estimates for how the coefficient may vary a priori with operating condition. For example, we note that increases in propellant mass (Fig. 9 a) $\rightarrow$ b)), discharge voltage (Fig. 9 b) $\rightarrow$ d)), and discharge current (Fig. 9 a) $\rightarrow$ c)) all result in a decrease in the scaling coefficient. We revisit these trends in Sec.VIII.

Although the calibrated model exhibits agreement with the ion velocity profiles, we note that these tuned conditions still underpredict (for most cases) the electron temperature in the same way as for the 300 V and 15 A case on krypton.

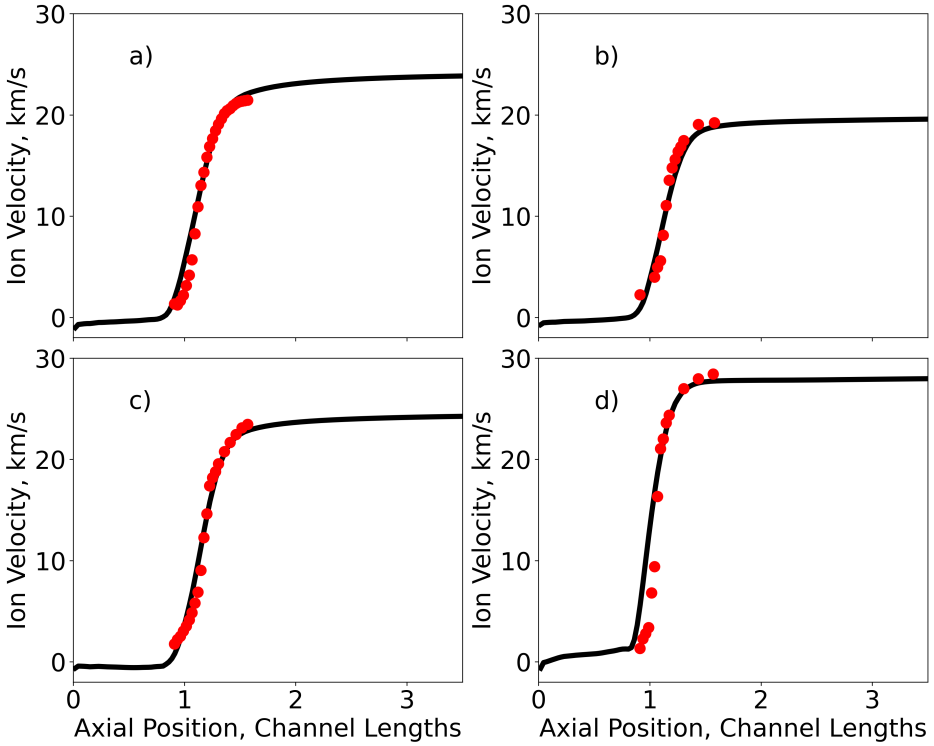

Fig. 9 Ion Velocity Along Channel Centerline for Various Operating Conditions. a) krypton at 300V 15A with c=1000, b) xenon at 300V 15A with c=640, c) krypton at 300V 30A with c=250, d) xenon at 600V 15A with c=500.

Fig. 10 illustrates this result where we see that while the shape of the temperature profile is qualitatively correct for Figs. 10(a)-(c), the magnitude of the peak is too low. There is one exception to this trend, 10(d), where we see that the simulation exhibits a peak that exceeds the measured electron temperature. To explain this discrepancy, we note that it has been demonstrated in a series of previous experiments [59] that higher discharge voltages translate to an upstream shift in the plasma profiles in Hall thrusters. It is thus possible that the peak temperature in the experiment has shifted to a region upstream of where we could access it with our diagnostics. If the peak is indeed upstream, it would not be possible to draw a definitive conclusion about the over or underprediction of the model.

C. Summary

In this section we have explored the implications of adjusting the the scaling of the coefficient in our anomalous collision frequency (Eq. 8) on the response of the plasma simulation. While we have found that by varying only a single parameter, we can make the simulation match key aspects of the internal plasma dynamics, this same value does not yield a commensurate prediction of a key global property, the discharge current. This points to a possible failing of the model. We similarly have found that by adjusting the value of c, we can identify calibrated profiles that are able to extend over multiple discharge voltages, currents, and propellants, though as was the case in the previous section, the temperatures are underpredicted for all conditions. This result suggest that the current scaling captures some, but not all, of the dependence of the anomalous collision frequency on local plasma profiles and is further discussed in Sec. VIII.

VIII. Discussion

In this section, we first discuss the performance of the free-stream heat flux on centerline properties. We then turn to the two-dimensional behavior along a magnetic field line. We follow with an interpretation of the physical mechanisms behind our best performing heat flux model. We conclude the heat flux discussion with regards to further adjustments of our model coefficients. We then detail the success and limitations of the scaled electron ion collision frequency closure for the anomalous collision frequency. Finally, we provide insight into the model extensibility and future modifications

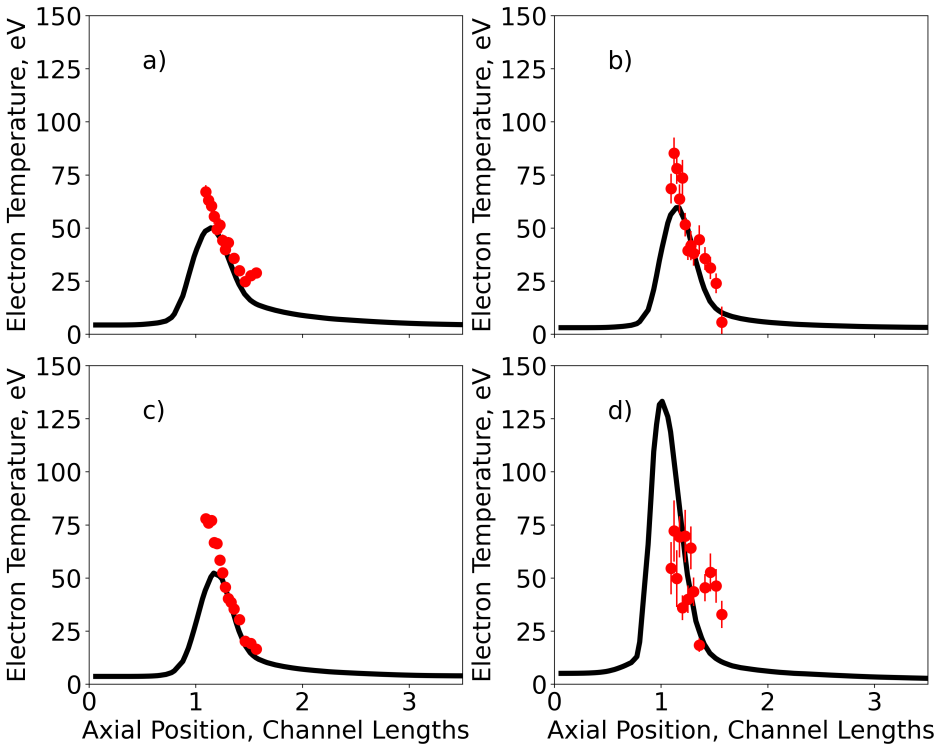

Fig. 10 Electron temperature along channel centerline for various operating conditions. a) krypton at 300V 15A with c=1000, b) xenon at 300V 15A with c=640, c) krypton at 300V 30A with c=250, d) xenon at 600V 15A with c=500.

to our self-consistent closure.

A. Physical significance of relationship between heat flux closures and peak electron temperature

As shown in Fig. 4 b) and discussed in the previous sections, a key finding of this work is that that the dominant driver for the electron temperature does not appear to be the choice of heat flux model but rather the factor modifying wall losses. This is physically intuitive as the walls represent the boundary condition for heat flux, controlling the degree to which internal energy can escape the system. The rate at which heat can escape along field lines to these boundary conditions does have some influence on temperature. We have shown, for example, that the convective heat flux models, which allow for less parallel transport, do lead to marginally higher electron temperatures in the discharge. However, this effect is small compared to the wall losses. From a physical perspective, this dominance of the wall losses may point to the fact that the processes in these regions may need to be revisited rigorously to illuminate from first principles how our conventional understanding of the sheath physics may be in error for the Hall thruster boundary conditions. As we have discussed to in previous work (Ref. [35]), the presence of strong magnetic field may be a key factor driving this.

With that said, regardless of wall loss factor or heat flux, our results were unable to recreate the maximum values of temperature we observed experimentally. This result suggests we continue to overestimate the loss of energy to the walls. One strategy to address this discrepancy could be to continue to lower the wall losses, though we have in practice found that using values below 0.01 leads to numerical instability that collapses the discharge. As an alternative, our finding may suggest that we are underestimating Ohmic heating in the discharge. This hypothesis is supported by the fact that we have found consistently that our anomalous collision frequencies are too high–and by extension our electric field magnitudes are too low. This idea would suggest that the low temperature results may in part be ameliorated by a reconsideration of our model of the anomalous collision frequency.

B. Physical significance of relationship between heat flux closures and temperature distribution along field lines

While our results would indicate that the magnitude of the temperature is primarily driven by wall losses and Ohmic heating rather than the parallel heat flux model, we have found that the heat flux models differ markedly in the predicted temperatures along field lines. In particular, as we noted in Sec. VI, the free-stream flux models are able to capture the two-dimensional behavior of electron properties along field lines in a way that the SH model does not.

Physically, the reason that the SH model fails can be seen from Eq. 10 where the parallel conductivity is inversely dependent upon the electron collision frequency. If the collisionality becomes low, as indicated by measurements along field lines in Hall thrusters [36], the SH heat flux will become large. This sizable heat flux rapidly transports electron energy along field lines, causing them to be isothermal. In contrast, the free-stream fluxes are largely independent of collision frequency and thus have reduced thermal transport along field lines (by up to two orders of magnitude). This reduced heat flux allows for spatial variation in electron temperature, which is consistent with our experimental measurement.

C. Physical significance of why the convective thermal heat flux model has best performance

As we have outlined in Sec. II, our choice to investigate heat flux models that are based on convection is inspired by the fact that the underlying assumptions of the SH model, i.e. that collisions are dominant in the parallel direction, are violated in the thruster. We in turn have looked to adjacent fields of plasma physics for inspiration for alternative heat flux models to explore.

In practice, we have found that the free-streaming heat flux model that uses a thermal velocity but with the heat flux directed in the direction of the average electron velocity yields the best agreement with experiment. The fact that this model depends on the magnitude of the thermal velocity is not surprising given that the bulk motion of electrons along fields is expected to negligible compared to the thermal speed (which contrasts with many types of space-plasma plasmas where the bulk electron velocity parallel to field lines is supersonic). With that said, it is not immediately clear why the heat flux should follow the direction of the bulk velocity.

One qualitative explanation for this may stem from considering the actual derivation of the heat flux, which depends on the skewness (third statistical moment) of the distribution function. In the case where the electron mean free path exceeds the characteristic length of the discharge, we do not expect a priori the electron velocity distribution to be thermalized. It is rather likely a result of non-localized effects as electrons approach the thruster wall along field lines and are either absorbed or reflected by the sheath. In this way, we may qualitatively expect the local distribution function to exhibit features that include a net motion toward the walls and a skewness in the same direction. In the context of the heat flux, these features could result in a distribution that depends on the characteristic speed of the electrons (the thermal speed) as well as the bulk motion, which is indeed the feature we see here.

With that said, the reason that this closure is better than the others remains an open question and invites follow-on investigations into what factors may drive non-local features of the EVDF and in turn how these may impact fluid-based estimates for the heat flux.

D. Effects on model-based approach stemming from non-exhaustive search of parameter space

In sections VI and VII we only explored the variation in coefficients independently. Mathematically, it is therefore possible that our approach missed the optimal set of coefficients for capturing the centerline properties. Physically, however, it is unlikely that a rigorous search of the three-dimensional parameter space (c, α, c_w) will return a better result. As mentioned above, different forms of the free-stream flux result in marginal gains to the peak energy and the thermal velocity along field lines is orders of magnitude higher than the bulk velocity. This result implies that further reduction to the parallel heat flux would be unable to concentrate sufficient energy on centerline to produce the observed temperature. As for the wall loss coefficient, the aforementioned collapse of the discharge at values of $c_w < 0.01$ imposes a lower bound on the wall losses. As increasing the value of c_w results in lower peak temperatures, we consider the $c_w = 0.01$ to be a near optimal value. Therefore, with both energy parameters expected to currently provide the best match, we do not expect further search to yield a better set of coefficients.

E. Limitations and extensions of anomalous collision frequency model

A key finding from our analysis is that it possible to nearly re-create the steep ion acceleration in the Hall thruster with a self-consistent closure model that depends on background plasma properties. As we have discussed in Sec. II, this result is in large part enabled by the fact that the higher electron temperatures in the thruster discharge allow for

more relaxed spital variation in collision frequency while still promoting large amplitude electric fields.

Our dependencies on local properties in our collision frequency profile is also a key enabling feature for being able to exhibit qualitative agreement with experimental data. In particular, the existence of a minimum in the collision frequency profile is key to capture the steep electric field and ion acceleration[31]. Physically, the inverse dependence of the model on temperature (Eq. 8) creates a dip in the collision frequency profile, in agreement with calibrated models. As the electron heating in Hall thrusters is driven by Ohmic heating, the temperature should peak near the peak electric field. This self-consistent mechanism is what correctly places the electric field: the peak in the temperature creates a stronger electric field through a minimum in the collision frequency, which further heats the electrons, creating a steeper dip in a cycle that continues until heating is balanced out by the convective and heat fluxes.

Despite the success of the electric field placement and steepness, there are notable limitations to this model. Figure 4 displays two key limitations: 1. the peak temperature is 25% lower than the measured value and 2. the simulated ion velocity profile does not match within experimental error near the channel exit. These discrepancies both point to the fact that the electric fields in the channel are too low, which is in turn can be explained by the fact that the minimum in collision frequency is a factor of five higher than the experimental measurement (Fig. 4 d).

This invites the question if there are modifications to this simplified closure that could self-consistently produce a more precipitous decrease in collision frequency.

To this end, one possible modification is to the linear dependence of the model on the electron number density. Figure 2 shows how the electron number density is high in the channel, which then drives the anomalous collision frequency in the channel upwards. As the electric field is inversely dependent upon the collision frequency, an erroneously high collision frequency in the channel would artificially lower the electric field in the channel. In turn, this effect would lower the Ohmic heating and thus the electron temperature. Modifying the dependence of the model on density by inverting or eliminating it entirely may help bring the model in line with experiment. As an alternative, models that have a stronger dependence in the electron temperature (for example, an inverse quadratic scaling) may yield an improved agreement. These modifications are the subject of on-going investigations.

F. Insight into extensibility of anomalous collision frequency

As a final consideration, we remark here that as we showed in the preceding section, we are able to match the ion velocity profiles for the four operating conditions considered by adjusting only a single coefficient in our model. However, the need for this tuning the coefficient suggests that the anomalous collision frequency has additional dependencies on local plasma properties that are not captured by Eq. 8.

With that said, the trends exhibited in Fig. 9 with operating condition offer some interesting clues as to the nature of these missing dependencies. For example, the ratio of $\frac{c_{Xe}}{c_{Kr}}$ =0.64 between the xenon and krypton coefficients at the 300V 15A is in agreement with the ratio between the mass of krypton and xenon $\frac{m_{Kr}}{m_{Xe}} = 0.638$. This may suggest that we need to incorporate mass scaling into the model. The discharge current and voltage variation provide further motivation for the modifications suggested in the preceding section. As changing the discharge current increases the plasma density, the decrease in scaling coefficient with a higher current suggests that the model may need to depend inversely on the density. Likewise, the as voltage is increased, the electron temperature is expected to increase, so the slight decrease in coefficient supports stronger dependence on the electron temperature. Further investigation should also incorporate data from other operating conditions that were not employed here.

IX. Conclusion

In this work, we investigated parametrically the results of new closure forms of the anomalous collision frequency and electron heat flux in a multi-fluid model for a Hall thruster. Motivated by previous experimental studies, we have explored convective models or heat flux that effectively reduced heat transport along field lines. We also have examined a closure for the electron collision frequency based on a modified version of the electron-ion collision frequency. We have found that the updated model can match with a high degree fidelity the distribution of ion velocity along the channel of a Hall thruster. The model in turn can capture the variation in electron temperature along a field line in the thruster. We also have shown shown the model is able to extend to prediction ion velocity profiles in other operating conditions by only adjusting a single tuning parameter. With that said, we have found our model underpredict electron temperatures, resulting in lower mass utilization. We have shown this is in large part due to the fact that the self-consistent estimates for collision frequency are too high in the region of peak magnetic field. We have discussed these results in the context of possible modifications to the heat flux and collision frequency that could inform improved agreement in the future.

Indeed, more broadly, this work has implications on the field as it demonstrates how modifications to the electron energy closure informed by experimental measurements of electron properties can enable simple, self-consistent closures of anomalous transport.

Acknowledgments

This work was supported in part by a NSF GRFP, the NASA Joint Advance Propulsion Institute (80NSSC21K1118), and in part through computational resources and services provided by Advanced Research Computing at the University of Michigan.

The authors would like to thank Dr. Ioannis Mikellides and Dr. Alejandro Lopez Ortega at the Jet Propulsion Laboratory for allowing the use of Hall2De. We would also like to thank Madison Allen and Ari Ekhaus for insightful discussion and comments on the manuscript.

References

[1] Hara, K., and Hanquist, K., "Test cases for grid-based direct kinetic modeling of plasma flows," *Plasma Sources Science and Technology*, Vol. 27, No. 6, 2018, p. 065004. https://doi.org/10.1088/1361-6595/aac6b9, URL https://dx.doi.org/10.1088/1361-6595/aac6b9.

[2] Boeuf, J.-P., "Tutorial: Physics and modeling of Hall thrusters," *Journal of Applied Physics*, Vol. 121, No. 1, 2017, p. 011101. https://doi.org/10.1063/1.4972269, URL https://doi.org/10.1063/1.4972269.

[3] Villafana, W., Powis, A., Kaganovich, I., Khrabov, A., Etheir, S., Sydorenko, D., and Chen, J., "Algorithms and High-Performance Computing for Kinetic Electric Propulsion Simulations," *38th International Electric Propulsion Conference*, Electric Rocket Propulsion Society, Toulouse, France, 2024. URL https://electricrocket.org/IEPC_2024/748.pdf, paper no. 748.

[4] Taccogna, F., and Garrigues, L., "Latest progress in Hall thrusters plasma modelling," *Rev. Mod. Plasma Phys.*, Vol. 3, No. 12, 2019. https://doi.org/https://doi.org/10.1007/s41614-019-0033-1, URL https://link.springer.com/article/10.1007/s41614-019-0033-1.

[5] Davidson, R., and Krall, N., "Anomalous transport in high-temperature plasmas with applications to solenoidal fusion systems," *Nuclear Fusion*, Vol. 17, No. 6, 1977, p. 1313. https://doi.org/10.1088/0029-5515/17/6/017, URL https://dx.doi.org/10.1088/0029-5515/17/6/017.

[6] Mikellides, I. G., and Katz, I., "Numerical simulations of Hall-effect plasma accelerators on a magnetic-field-aligned mesh," *Phys. Rev. E*, Vol. 86, 2012, p. 046703. https://doi.org/10.1103/PhysRevE.86.046703, URL https://link.aps.org/doi/10.1103/PhysRevE.86.046703.

[7] Morozov, A. I., and Savel'ev, V., "One-Dimensional hybrid model of a stationary plasma thruster," *Plasma Phys. Rep.*, Vol. 26, 2000, pp. 875–880.

[8] Ahedo, E., Gallardo, J. M., and Martinez-Sanchez, M., "Model of the plasma discharge in a Hall thruster with heat conduction," *Physics of Plasmas*, Vol. 9, No. 9, 2002, pp. 4061–4070. https://doi.org/10.1063/1.1499496, URL https://doi.org/10.1063/1.1499496.

[9] Hagelaar, G. J. M., Bareilles, J., Garrigues, L., and Boeuf, J. P., "Two-dimensional model of a stationary plasma thruster," *Journal of Applied Physics*, Vol. 91, No. 9, 2002, pp. 5592–5598. https://doi.org/10.1063/1.1465125, URL https://doi.org/10.1063/1.1465125.

[10] Parra, F. I., Ahedo, E., Fife, J. M., and Martínez-Sánchez, M., "A two-dimensional hybrid model of the Hall thruster discharge," *Journal of Applied Physics*, Vol. 100, No. 2, 2006, p. 023304. https://doi.org/10.1063/1.2219165, URL https://doi.org/10.1063/1.2219165.

[11] Sahu, R., Mansour, A. R., and Hara, K., "Full fluid moment model for low temperature magnetized plasmas," *Physics of Plasmas*, Vol. 27, No. 11, 2020, p. 113505. https://doi.org/10.1063/5.0021474, URL https://doi.org/10.1063/5.0021474.

[12] Domínguez-Vázquez, A., "Axisymmetric simulation codes for Hall effect thrusters and plasma plumes," Ph.D. thesis, Universidad Carlos III de Madrid, 2019.

[13] Poli, D., Bello-Benítez, E., Fajardo, P., and Ahedo, E., "Time-dependent axial fluid model of the Hall thruster discharge and its plume," *Journal of Physics D: Applied Physics*, Vol. 56, No. 41, 2023, p. 415203. https://doi.org/10.1088/1361-6463/ace2d0, URL https://dx.doi.org/10.1088/1361-6463/ace2d0.

[14] Shashkov, A., Lovtsov, A., Tomilin, D., and Kravchenko, D., "Numerical study of viscosity and heat flux role in heavy species dynamics in Hall thruster discharge," *Plasma Science and Technology*, Vol. 25, No. 1, 2022, p. 015511. https://doi.org/10.1088/2058-6272/ac82e0, URL https://dx.doi.org/10.1088/2058-6272/ac82e0.

[15] Fife, J. M., "Hybrid-PIC Modeling and Electrostatic Probe Survey of Hall Thruster," Ph.D. thesis, Massachusetts Institute of Technology, 1998.

[16] Hofer, R., Katz, I., Goebel, D., Jameson, K., Sullivan, R., Johnson, L., and Mikellides, I., "Efficacy of Electron Mobility Models in Hybrid-PIC Hall Thruster Simulations," *44th AIAA/ASME/SAE/ASEE Joint Propulsion Conference*, 2008. https://doi.org/10.2514/6.2008-4924, URL https://arc.aiaa.org/doi/abs/10.2514/6.2008-4924.

[17] Mikellides, I. G., and Lopez Ortega, A., "Challenges in the development and verification of first-principles models in Hall-effect thruster simulations that are based on anomalous resistivity and generalized Ohm's law*," *Plasma Sources Science and Technology*, Vol. 28, No. 1, 2019, p. 014003. https://doi.org/10.1088/1361-6595/aae63b, URL https://dx.doi.org/10.1088/1361-6595/aae63b.

[18] Mikellides, I. G., Katz, I., Hofer, R. R., and Goebel, D. M., "Magnetic shielding of a laboratory Hall thruster. I. Theory and validation," *Journal of Applied Physics*, Vol. 115, No. 4, 2014, p. 043303. https://doi.org/10.1063/1.4862313, URL https://doi.org/10.1063/1.4862313.

[19] Morozov, A. I., and Savel'ev, V. V., *Reviews of Plasma Physics*, Vol. 21, Kluwe Academic/Plenum Publisers, 2000.

[20] Boeuf, J. P., and Garrigues, L., "Low frequency oscillations in a stationary plasma thruster," *Journal of Applied Physics*, Vol. 84, No. 7, 1998, pp. 3541–3554. https://doi.org/10.1063/1.368529, URL https://doi.org/10.1063/1.368529.

[21] Cappelli, M., Meezan, N., and Gascon, N., "Transport physics in Hall plasma thrusters," 2002. https://doi.org/10.2514/6.2002-485, URL https://arc.aiaa.org/doi/abs/10.2514/6.2002-485.

[22] Scharfe, M. K., Thomas, C. A., Scharfe, D. B., Gascon, N., Cappelli, M. A., and Fernandez, E., "Shear-Based Model for Electron Transport in Hybrid Hall Thruster Simulations," *IEEE Transactions on Plasma Science*, Vol. 36, No. 5, 2008, pp. 2058–2068. https://doi.org/10.1109/TPS.2008.2004364.

[23] Chodura, R., Bardotti, G., and Engelmann, F., "Numerical investigation of the anomalous resistivity due to two-stream instability," *Plasma Physics*, Vol. 13, No. 12, 1971, p. 1099. https://doi.org/10.1088/0032-1028/13/12/002, URL https://dx.doi.org/10.1088/0032-1028/13/12/002.

[24] Cappelli, M. A., Young, C. V., Cha, E., and Fernandez, E., "A zero-equation turbulence model for two-dimensional hybrid Hall thruster simulations," *Physics of Plasmas*, Vol. 22, No. 11, 2015, p. 114505. https://doi.org/10.1063/1.4935891, URL https://doi.org/10.1063/1.4935891.

[25] Jorns, B. A., "Two Equation Closure Model for Plasma Turbulence in a Hall Effect Thruster," *36th International Electric Propulsion Conference*, Electric Rocket Propulsion Society, Vienna, Austria, 2019. URL https://pepl.engin.umich.edu/pdf/IEPC-2019-129.pdf.

[26] Mikellides, I. G., Jorns, B., Katz, I., and Ortega, A. L., *Hall2De Simulations with a First-principles Electron Transport Model Based on the Electron Cyclotron Drift Instability*, 2016. https://doi.org/10.2514/6.2016-4618, URL https://arc.aiaa.org/doi/abs/10.2514/6.2016-4618.

[27] Mikellides, I. G., Lopez Ortega, A., and Chaplin, V. H., "Theory of the anomalous momentum exchange from wave–particle interactions in Hall-effect ion accelerators and comparisons with measurements," *Physics of Fluids*, Vol. 36, No. 7, 2024, p. 074121. https://doi.org/10.1063/5.0213605, URL https://doi.org/10.1063/5.0213605.

[28] Lafleur, T., Baalrud, S. D., and Chabert, P., "Theory for the anomalous electron transport in Hall effect thrusters. II. Kinetic model," *Physics of Plasmas*, Vol. 23, No. 5, 2016, p. 053503. https://doi.org/10.1063/1.4948496, URL https://doi.org/10.1063/1.4948496.

[29] Marks, T. A., "Modeling Anomalous Electron Transport in a Fluid Hall Thruster Code," Ph.D. thesis, University of Michigan, 2023.

[30] Su, L. L., Marks, T. A., and Jorns, B. A., "Investigation into the Efficiency Gap between Krypton and Xenon Operation on a Magnetically Shielded Hall Thruster," *37th International Electric Propulsion Conference*, Electric Rocket Propulsion Society, Boston, USA, 2022. URL https://www.jotform.com/uploads/electricrocket/220994246997171/531481189241654505 9/IEPC_2022_Su_L_Krypton.pdf.

[31] Marks, T. A., and Jorns, B. A., "Evaluation of algebraic models of anomalous transport in a multi-fluid Hall thruster code," *Journal of Applied Physics*, Vol. 134, No. 15, 2023, p. 153301. https://doi.org/10.1063/5.0171824, URL https://doi.org/10.1063/5.0171824.

[32] Roberts, P. J., and Jorns, B., *Inferring Electron Heat Flux in a High-Power Hall Thruster with Incoherent Thomson Scattering*, 2024. https://doi.org/10.2514/6.2024-1957, URL https://arc.aiaa.org/doi/abs/10.2514/6.2024-1957.

[33] Lopez-Uricoechea, J., Suazo Betancourt, J. L., Butler-Craig, N., and Walker, M. L., "Laser Thomson Scattering Measurements and Inference of the Electron Hall Parameter Across the Acceleration Region of a Hall Effect Thruster," *38th International Electric Propulsion Conference*, Electric Rocket Propulsion Society, Toulouse, France, 2024. URL https://electricrocket.org/IEPC_2024/509.pdf, paper no. 509.

[34] Roberts, P. J., and Jorns, B. A., "Laser Measurement of Anomalous Electron Diffusion in a Crossed-Field Plasma," *Phys. Rev. Lett.*, Vol. 132, 2024, p. 135301. https://doi.org/10.1103/PhysRevLett.132.135301, URL https://link.aps.org/doi/10.1103/PhysRevLett.132.135301.

[35] Brick, D., Roberts, P. J., and Jorns, B. A., "Model Based Investigation of Anomalous Energy Transport in a Magnetically-Shielded Hall Thruster," *38th International Electric Propulsion Conference*, Electric Rocket Propulsion Society, Toulouse, France, 2024. URL https://electricrocket.org/IEPC_2024/411.pdf, paper no. 411.

[36] Roberts, P. J., Allen, M. G., and Jorns, B. A., "Thomson Scattering Investigations of Hall Thruster Anomalous Electron Transport," *38th International Electric Propulsion Conference*, Electric Rocket Propulsion Society, Toulouse, France, 2024. URL https://electricrocket.org/IEPC_2024/393.pdf, paper no. 393.

[37] Betancourt, J. L. S., Butler-Craig, N., Lopez-Uricoechea, J., Steinberg, A. M., and Walker, M. L. R., "Laser Thomson scattering measurements indicate non-isothermal magnetic field lines in magnetically shielded Hall effect thrusters," *Physics of Plasmas*, Vol. 31, No. 11, 2024, p. 113106. https://doi.org/10.1063/5.0229827, URL https://doi.org/10.1063/5.0229827.

[38] Tsikata, S., Hara, K., and Dubois, T., "Insights from combined optical diagnostics and numerical analyses of Hall thruster turbulence," *38th International Electric Propulsion Conference*, Electric Rocket Propulsion Society, Toulouse, France, 2024. URL https://electricrocket.org/IEPC_2024/862.pdf, paper no. 862.

[39] Marks, T., Schedler, P., and Jorns, B., "HallThruster.jl: a Julia package for 1D Hall thruster discharge simulation," *Journal of Open Source Software*, Vol. 8, No. 86, 2023, p. 4672. https://doi.org/10.21105/joss.04672, URL https://doi.org/10.21105/joss.04672.

[40] Spitzer, L., and Harm, R., "Transport Phenomena in a Completely Ionized Gas," *Phys. Rev.*, Vol. 89, 1953, pp. 977–981. https://doi.org/10.1103/PhysRev.89.977, URL https://link.aps.org/doi/10.1103/PhysRev.89.977.

[41] Richardson, A., *NRL plasma formulary*, Naval Research Lab., Washington, DC, 2019. URL https://library.psfc.mit.edu/catalog/online_pubs/NRL_FORMULARY_19.pdf.

[42] Dragnea, H. C., Ortega, A. L., Kamhawi, H., and Boyd, I. D., "Simulation of a Hall Effect Thruster Using Krypton Propellant," *Journal of Propulsion and Power*, Vol. 36, No. 3, 2020, pp. 335–345. https://doi.org/10.2514/1.B37499, URL https://doi.org/10.2514/1.B37499.

[43] Braginskii, S., "Transport Processes in a Plasma," *Reviews of Plasma Physics*, Vol. 1, 1965, pp. 205–311. URL https://static.ias.edu/pitp/2016/sites/pitp/files/braginskii_1965-1.pdf.

[44] Arber, T. D., Goffrey, T., and Ridgers, C., "Models of thermal conduction and non-local transport of relevance to space physics with insights from laser–plasma theory," *Frontiers in Astronomy and Space Sciences*, Vol. 10, 2023. https://doi.org/10.3389/fspas.2023.1155124, URL https://www.frontiersin.org/journals/astronomy-and-space-sciences/articles/10.3389/fspas.2023.1155124.

[45] van der Holst, B., Sokolov, I. V., Meng, X., Jin, M., W. B. Manchester, I., Tóth, G., and Gombosi, T. I., "ALFVÉN WAVE SOLAR MODEL (AWSoM): CORONAL HEATING," *The Astrophysical Journal*, Vol. 782, No. 2, 2014, p. 81. https://doi.org/10.1088/0004-637X/782/2/81, URL https://dx.doi.org/10.1088/0004-637X/782/2/81.

[46] Hollweg, J. V., "Collisionless electron heat conduction in the solar wind," *Journal of Geophysical Research (1896-1977)*, Vol. 81, No. 10, 1976, pp. 1649–1658. https://doi.org/https://doi.org/10.1029/JA081i010p01649, URL https://agupubs.onlinelibrary.wiley.com/doi/abs/10.1029/JA081i010p01649.

[47] Fundamenski, W., "Parallel heat flux limits in the tokamak scrape-off layer," *Plasma Physics and Controlled Fusion*, Vol. 47, No. 11, 2005, p. R163. https://doi.org/10.1088/0741-3335/47/11/R01, URL https://dx.doi.org/10.1088/0741-3335/47/11/R01.

[48] Myers, J. L., Kamhawi, H., Yim, J., and Clayman, L., *Hall Thruster Thermal Modeling and Test Data Correlation*, 2016. https://doi.org/10.2514/6.2016-4535, URL https://arc.aiaa.org/doi/abs/10.2514/6.2016-4535.

[49] Keidar, M., and Beilis, I. I., "Sheath and boundary conditions for plasma simulations of a Hall thruster discharge with magnetic lenses," *Applied Physics Letters*, Vol. 94, No. 19, 2009, p. 191501. https://doi.org/10.1063/1.3132083, URL https://doi.org/10.1063/1.3132083.

[50] Katz, I., and Mikellides, I. G., "Neutral gas free molecular flow algorithm including ionization and walls for use in plasma simulations," *Journal of Computational Physics*, Vol. 230, No. 4, 2011, pp. 1454–1464. https://doi.org/https://doi.org/10.1016/j.jcp.2010.11.013, URL https://www.sciencedirect.com/science/article/pii/S0021999110006212.

[51] Lopez Ortega, A., and Mikellides, I. G., *A New Cell-Centered Implicit Numerical Scheme for Ions in the 2-D Axisymmetric Code Hall2De*, 2014. https://doi.org/10.2514/6.2014-3621, URL https://arc.aiaa.org/doi/abs/10.2514/6.2014-3621.

[52] Lopez Ortega, A., and Mikellides, I. G., "The importance of the cathode plume and its interactions with the ion beam in numerical simulations of Hall thrusters," *Physics of Plasmas*, Vol. 23, No. 4, 2016, p. 043515. https://doi.org/10.1063/1.4947554, URL https://doi.org/10.1063/1.4947554.

[53] Georgin, M. P., Jorns, B. A., and Gallimore, A. D., "Transient non-classical transport in the hollow cathode plume I: measurements of time-varying electron collision frequency," *Plasma Sources Science and Technology*, Vol. 29, No. 10, 2020, p. 105010. https://doi.org/10.1088/1361-6595/abb0ce, URL https://dx.doi.org/10.1088/1361-6595/abb0ce.

[54] Lopez Ortega, A., and Mikellides, I. G., "Erosion Mechanisms at the Outer Front Pole Cover of a Magnetically Shielded Hall Thruster," *38th International Electric Propulsion Conference*, Electric Rocket Propulsion Society, Toulouse, France, 2024. URL https://electricrocket.org/IEPC_2024/264.pdf, paper no. 264.

[55] Hofer, R. R., Cusson, S. E., Lobbia, R. B., and Gallimore, A. D., "The H9 Magnetically Shielded Hall Thruster," *35th International Electric Propulsion Conference*, Electric Rocket Propulsion Society, Atlanta, Georgia, 2017.

[56] Su, L. L., and Jorns, B. A., "Performance comparison of a 9-kW magnetically shielded Hall thruster operating on xenon and krypton," *Journal of Applied Physics*, Vol. 130, No. 16, 2021, p. 163306. https://doi.org/10.1063/5.0066849, URL https://doi.org/10.1063/5.0066849.

[57] Goebel, D. M., Katz, I., and Mikellides, I. G., *Fundamentals of Electric Propulsion: Ion and Hall Thrusters*, Jet Propulsion Laboratory, 2023.

[58] Lopez Ortega, A., and Mikellides, I. G., "2D Fluid-PIC Simulations of Hall Thrusters with Self-Consistent Resolution of the Space-Charge Regions," *Plasma*, Vol. 6, No. 3, 2023, pp. 550–562. https://doi.org/10.3390/plasma6030038, URL https://www.mdpi.com/2571-6182/6/3/38.

[59] Chaplin, V. H., Jorns, B. A., Lopez Ortega, A., Mikellides, I. G., Conversano, R. W., Lobbia, R. B., and Hofer, R. R., "Laser-induced fluorescence measurements of acceleration zone scaling in the 12.5 kW HERMeS Hall thruster," *Journal of Applied Physics*, Vol. 124, No. 18, 2018, p. 183302. https://doi.org/10.1063/1.5040388, URL https://doi.org/10.1063/1.5040388.